Ceramics International xxx (xxxx) xxx

Contents lists available at ScienceDirect

Ceramics International

journal homepage: www.elsevier.com/locate/ceramint

Microwave dielectric and mechanical properties of high-entropy $Li_2(Mg_{0.2}Mn_{0.2}Co_{0.2}Ni_{0.2}Zn_{0.2})_2Mo_3O_{12}$ ceramics

Yutong Meng [a], Qi Yuan [b], Sen Wang [a,*]

[a] School of Materials and Metallurgy, University of Science and Technology Liaoning, Anshan, 114051, China
[b] College of Electronics and Information Engineering, Hangzhou Dianzi University, Hangzhou, 310018, China

ARTICLE INFO

Handling Editor: Dr P. Vincenzini

Keywords:
ULTCC
High-entropy ceramics
Microwave dielectric properties
Mechanical properties

ABSTRACT

Novel high-entropy $Li_2(Mg_{0.2}Mn_{0.2}Co_{0.2}Ni_{0.2}Zn_{0.2})_2Mo_3O_{12}$ ceramics (LAM) were prepared by solid-phase reaction method. LAM ceramics have a pure phase with a single orthorhombic structure and a space group of *Pnma* (62). The grain size increases gradually with the increase of sintering temperature and the distribution of each solid solution element is uniform. The ceramic samples sintered at 625 °C have excellent microwave dielectric properties ($\varepsilon_r = 9.82 \pm 0.13$, $Q \times f = 20{,}514 \pm 261$ GHz, $\tau_f = -67.74 \pm 1.63$ ppm/°C) and are analyzed in conjunction with the P-V-L theory for microwave dielectric properties. In addition to this, the high entropy design increases the Vickers hardness and compressive strength of LAM ceramics to 4.54 ± 0.13 GPa and 441 ± 34 MPa, respectively.

1. Introduction

With the rapid development in the field of electronics and information technology, the demand for ceramic dielectric materials has risen dramatically, aiming at achieving product miniaturization, high packaging density, and reduced production costs [1,2]. In this context, low-temperature co-fired ceramic (LTCC) technology stands out as the main approach to realize solutions for high-density integrated wiring and packaging strategies, especially for system applications at high frequencies (typically ranging up to the microwave region) [3]. In order to further reduce cost and save energy, ultra-low temperature co-fired ceramic (ULTCC) technology has been developed based on LTCC technology [4]. ULTCC is sintered at temperatures lower than 700 °C, which enables matched co-firing with cheaper and more readily available metallic Al electrodes [5]. Ultra-low temperature co-fired ceramics (ULTCC) enable electronic components with both high performance and low cost, which is particularly suitable for the future generation of telecommunications [6].

Conventional ULTCC technology requires ceramics with low dielectric constant (ε_r, to improve the signal transmission rate), high quality factor ($Q \times f$, to reduce the power consumption of microwave devices) and near-zero temperature coefficient of resonance frequency (τ_f, to improve the temperature independence of microwave devices) [7–9]. The current commercial mainstream of LTCC and even ULTCC systems is based on the glass-ceramic system, and although glass-ceramic has a low sintering temperature, the microwave dielectric properties are relatively poor [10]. Chen et al. [11] prepared low-melting Na_2O-K_2O-SiO_2--B_2O_3-Al_2O_3-P_2O_5 glass by the fusion method and composite with quartz to prepare glass with a dielectric constant of 6.51, a loss of 8×10^{-3}, and a flexural strength of 82 MPa glass-ceramic. Gao et al. [12] prepared xZnO-(100-x) B_2O_3 (x = 45–64 mol%) microcrystalline glass for ULTCC by solid-phase reaction method. 55 ZnO-45 B_2O_3 glass-ceramics sintered for 5 h at 640 °C exhibited the best microwave dielectric properties $\varepsilon_r = 6.09$, $Q \times f = 20{,}389$ GHz, $\tau_f = 14$ ppm/°C and a Vickers hardness of 625 kgf/mm^2. Although they meet the ULTCC sintering temperature standard (Sintering temperature is abbreviated as ST, ST < 700 °C), their mechanical properties are far from those required for applications under extreme conditions. Molybdate system microwave dielectric materials have excellent microwave dielectric properties, but there are fewer ceramic types with sintering temperatures less than 700 °C [13–18]. $Li_2Mg_2Mo_3O_{12}$ ceramics have excellent microwave dielectric properties ($\varepsilon_r = 9.26$, $Q \times f = 58{,}583$ GHz, and $\tau_f = -51$ ppm/°C) and low sintering temperature (ST = 650 °C) to fulfill the performance requirements of ULTCC [19]. Nevertheless, $Li_2Mg_2Mo_3O_{12}$ ceramics also suffer from poor mechanical properties and are prone to mechanical failure when applied under extreme conditions [20]. Therefore, it is not enough for ULTCC materials applied under extreme conditions to have excellent microwave dielectric properties, but they should also have good

* Corresponding author.
E-mail address: wsenl@yeah.net (S. Wang).

https://doi.org/10.1016/j.ceramint.2025.05.213
Received 26 March 2025; Received in revised form 12 May 2025; Accepted 13 May 2025
Available online 13 May 2025
0272-8842/© 2025 Elsevier Ltd and Techna Group S.r.l. All rights are reserved, including those for text and data mining, AI training, and similar technologies.

mechanical properties to improve the reliability of the devices and prolong their service life.

In recent years, high-entropy ceramics have become a research hotspot in many fields such as energy storage, thermoelectricity and batteries because of their unique properties [21,22]. In addition to this, high entropy ceramics can improve mechanical properties by severe lattice distortion [23]. Corlett et al. [24] successfully prepared (Co, Cu, Mg, Ni, Zn)Al_2O_4 ceramics with Vickers hardness greater than 10 GPa by hot press sintering at 1375 °C. Lin et al. [25] prepared high entropy Sr$(La_{0.2}Nd_{0.2}Sm_{0.2}Eu_{0.2}Gd_{0.2})AlO_4$ ceramics with layered perovskite structure by using solid-phase reaction method, and utilized the high entropy effect to increase the compressive strength from 583 MPa to 1040 MPa. It can be seen that the high entropy effect can also effectively improve the mechanical properties of ceramics.

This study employs a high-entropy design to improve the mechanical properties of $Li_2Mg_2Mo_3O_{12}$ ceramics and enhance their reliability under extreme conditions. By calculating the ionic radius difference (ΔR) and the entropy value (ΔS_{site}), five types of A^{2+} ions (A = $Mg_{0.2}Mn_{0.2}Co_{0.2}Ni_{0.2}Zn_{0.2}$) were selected to occupy the Mg lattice sites (calculation formulas and results can be found in Eqs. S1-S2 and Table S1), thereby inducing lattice distortion to balance the microwave dielectric and mechanical properties.

2. Experimental

$Li_2(Mg_{0.2}Mn_{0.2}Co_{0.2}Ni_{0.2}Zn_{0.2})_2Mo_3O_{12}$ ceramics were prepared by a solid-phase method using Li_2CO_3, MgO, MnO, CoO, NiO, ZnO, and MoO_3 as raw materials with a purity of greater than 98.5 % (all the raw materials used were from Aladdin), and were weighed according to stoichiometry. The raw materials were ball milled for 6 h, dried, and then calcined at 500 °C for 6 h. The calcined powder was ball milled for another 6 h, dried, sieved, and added to PVB (Polyvinyl Butyral) for granulation (ball milling media: ZrO_2, ball weight ratio of 8:1, rotation speed 450 rpm). The granulated powder was then pressed into cylindrical billets with a diameter of 12.7 mm and a thickness of 7 mm at a pressure of 5 MPa, and put into a vacuum-sealed bag and subjected to a cold isostatic pressure of 200 MPa. Finally, the sintering was carried out for 3 h at 575–675 °C.

The density of the ceramic samples was determined by Archimedes' method and the results are shown in Table S1. The crystalline phases of the ceramic samples were detected by X-ray diffraction (XRD, Cu Kα-radiation, 40 mA, 40 mV, 0.01°, 2θ = 10°–70°, Bruker), and use GXAS-II software to perform Rietveld refinement on XRD data to obtain lattice parameter information. The theoretical density (ρ_{th}) of the ceramic samples was calculated by bringing the calculated cell volume into Eq. (1):

$$\rho_{th} = \frac{AZ}{VN} \tag{1}$$

where A is the relative atomic mass, Z is the number of atoms in the single cell, V is the volume of the cell, and N is Avogadro's constant. The relative density (ρ_{rel}) were then calculated by combining Eq. (2):

$$\rho_{rel} = \frac{\rho_{bu}}{\rho_{th}} \tag{2}$$

ρ_{bu} and ρ_{rel} are the bulk density and relative density of the ceramic samples, respectively. The microstructure of the ceramic samples was examined using a scanning electron microscope (SEM, Zeiss, Oberkochen, Germany) and the grain size of the ceramics was counted using the Nano Measurer software. The microwave dielectric properties of the samples were tested by an Agilent Keysight E5063A network analyzer with resonance frequencies between 11.3 and 12.5 GH, and the τ_f of the ceramics was calculated by the following equation:

$$\tau_f = \frac{f_{T2} - f_{T1}}{f_{T1}(T_2 - T_1)} \tag{3}$$

where f_{T1} and f_{T2} denote the resonant frequencies at T_1 (25 °C) and T_2 (85 °C).

3. Results and discussion

The XRD detection results of LAM ceramics at each sintering temperature are shown in Fig. 1. It can be observed that the LAM ceramics assay results at each sintering temperature coincide with the $Li_2Mg_2Mo_3O_{12}$ standard PDF card, which all show a single orthorhombic phase structure. Fig. 1(b) shows that the strongest diffraction peaks of LAM ceramics show a left-right swaying shift with increasing sintering temperature, which suggests that the cell volume of LAM ceramics exhibits an increasing-shrinking floating change with increasing sintering temperature. In Fig. 1(c) of the LAM structure, A^{2+} and Li^+ are distributed in a variety of coordination environments, including low-symmetry $[Li_{0.341}/A_{0.659}O_6]1$ and highly distorted $[Li_{0.471}/A_{0.529}O_6]2$ octahedral centers (8d and 4c Wyckoff loci) as well as edge-sharing triangular prisms $[Li_{0.21}/A_{0.79}O_6]3$ (4c Wyckoff loci). Mo^{6+} occupies two different $[MoO_4]$ tetrahedral centers (4c and 8d Wyckoff point positions), and each $[MoO_4]$ tetrahedron is connected to three different $[Li/AO_6]$ polyhedra [19]. To further investigate the crystal structure of the high-entropy ceramics at each sintering temperature, the XRD data were subjected to Rietveld refinement to obtain the lattice parameters and theoretical densities (Table 1). The cell volume increases gradually with the sintering temperature, but the cell volume of the ceramic samples decreases abnormally when the sintering temperature reaches 675 °C. Fig. 3(f) also shows a small amount of amorphous or poorly crystallized microparticles at grain boundaries, further demonstrating the precipitation of Li [26]. A^{2+} and Li^+ occupy the polyhedral centers together, and the ionic radius of Li^+ (CN = 6, r = 0.76 Å) is larger than the A^{2+} ion average radius (CN = 6, r_{ave} = 0.694 Å) [27], the Li^+ ion content decreases, and the polyhedral volume decreases accordingly, resulting in a lower cell volume.

Fig. 2(a–e) shows the microscopic morphology of LAM ceramics at each sintering temperature (Fig. S1 shows the statistical data of grain size), and Fig. 2(f) shows the variation of the average grain size with sintering temperature. It can be found that the sintering is more dense and the grain size increases gradually with the sintering temperature. When the sintering temperatures (ST) were 575 °C and 675 °C, significant porosity was present in the ceramic samples. At 575 °C, the presence of porosity is mainly attributed to the low sintering temperature which does not meet the densification requirement, while at 675 °C, the presence of porosity is mainly attributed to the high sintering temperature which causes the billet to be overcooked. Fig. 2(f) shows that the average grain size increases abnormally at 675 °C, which further proves that the sintering temperature is too high, resulting in secondary recrystallization of LAM ceramics.

To further verify the uniformity of the distribution of each solid-solution element, EDS energy spectroscopy was performed on the ceramic samples sintered at 625 °C, and the results are shown in Fig. 3. Fig. 3(b) shows that the distribution of each element is uniform without obvious aggregation and segregation.

To further investigate the influence of intrinsic factors on the microwave dielectric properties of LAM ceramics, we use the P-V-L theory to calculate the ionicity (f_i) and lattice energy (U) of the bonds and discuss the influence of both on the microwave dielectric properties of ceramics. The complex bond decomposition theory was first utilized to decompose LAM into the following dibond expression [28]:

$Li_2A_2Mo_3O_{12}$=Li/A(1)$_{1/3}$O(1)$_{2/3}$+Li/A(1)$_{1/3}$O(3)$^1_{2/3}$+Li/A(1)$_{1/3}$O(3)$^2_{2/3}$+Li/A(1)$_{1/3}$O(4)$_{2/3}$+Li/A(1)$_{1/3}$O(6)$^1_{2/3}$+Li/A(1)$_{1/3}$O(6)$^2_{2/3}$+Li/A(2)$_{1/6}$O(2)$^1_{1/3}$+Li/A(2)$_{1/6}$O(2)$^2_{1/3}$+Li/A(2)$_{1/6}$O(5)1$_{1/3}$+Li/A(2)$_{1/6}$O(5)$^2_{1/3}$+Li/A(3)$_{1/3}$O(1)$_{2/3}$+Li/A(3)$_{1/3}$O(7)$^1_{2/3}$+Li/A(3)$_{1/3}$O(7)$^2_{2/3}$+Mo(1)$_{1/4}$O(2)$_{1/3}$+Mo(1)$_{1/2}$O(3)$_{2/3}$+Mo(1)$_{1/4}$O(4)$_{1/3}$+Mo(2)$_{1/2}$O(1)$_{2/3}$+Mo(2)$_{1/2}$O(5)$_{2/3}$+Mo(2)$_{1/2}$O(6)$_{2/3}$+Mo(2)$_{1/2}$O(7)$_{2/3}$

Calculations of f_i for LAM ceramics were carried out according to the

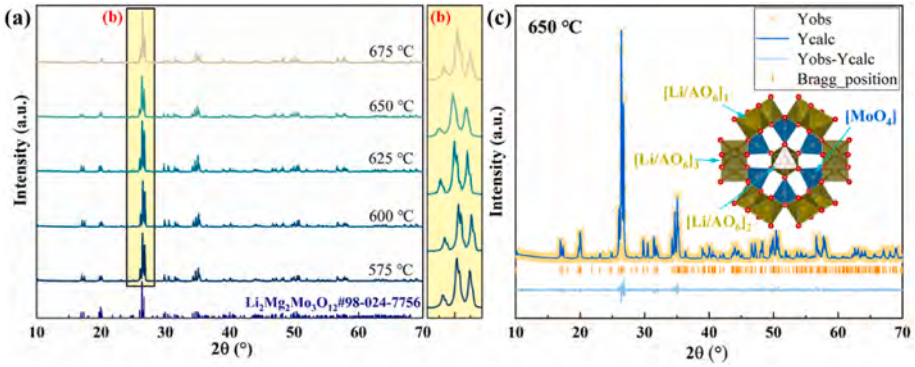

Fig. 1. (a) XRD spectra of LAM ceramics at various sintering temperatures, (b) magnification of the strongest diffraction peak of LAM ceramics, and (c) Rietveld refinement results of XRD data and schematic diagram of LAM crystal structure.

Table 1
Lattice parameters, theoretical density and bulk density of LAM ceramics at each sintering temperature.

ST (°C)	a (Å)	b (Å)	c (Å)	V (Å^3)	α = β = γ(°)	ρ_{th} (g·cm^{-3})	R_p (%)	R_{wp} (%)
575	5.12146	10.47995	17.61886	945.652	90	4.2060	7.3	9.8
600	5.12001	10.47801	17.61538	945.021	90	4.2088	6.1	8.3
625	5.12235	10.48216	17.62216	946.191	90	4.2036	6.8	8.8
650	5.12462	10.48730	17.63165	947.586	90	4.1974	7.4	9.3
675	5.11901	10.47501	17.61395	944.489	90	4.2112	6.9	9.1

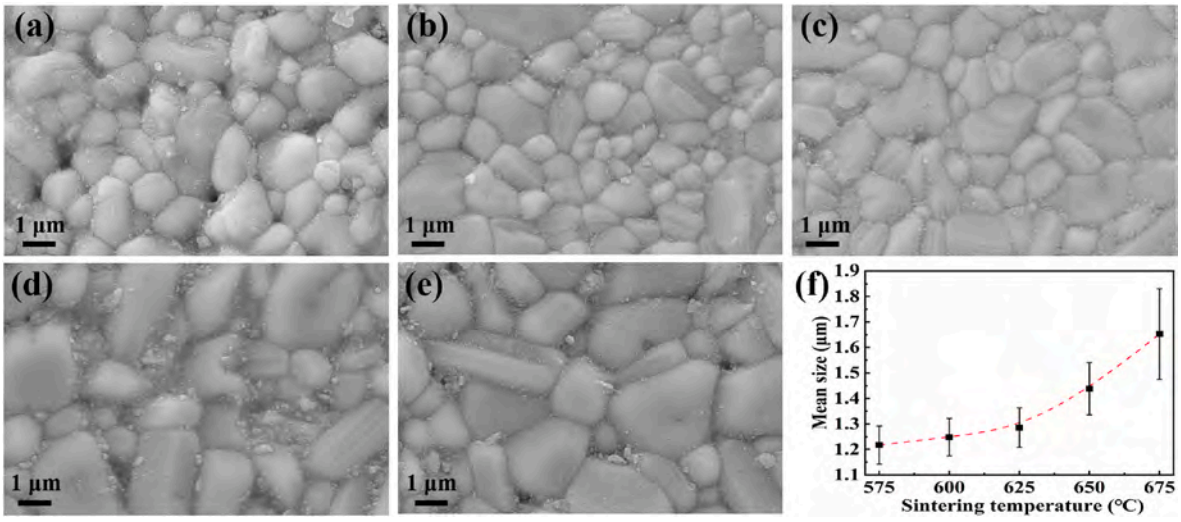

Fig. 2. SEM photographs of LAM ceramics at various sintering temperatures.

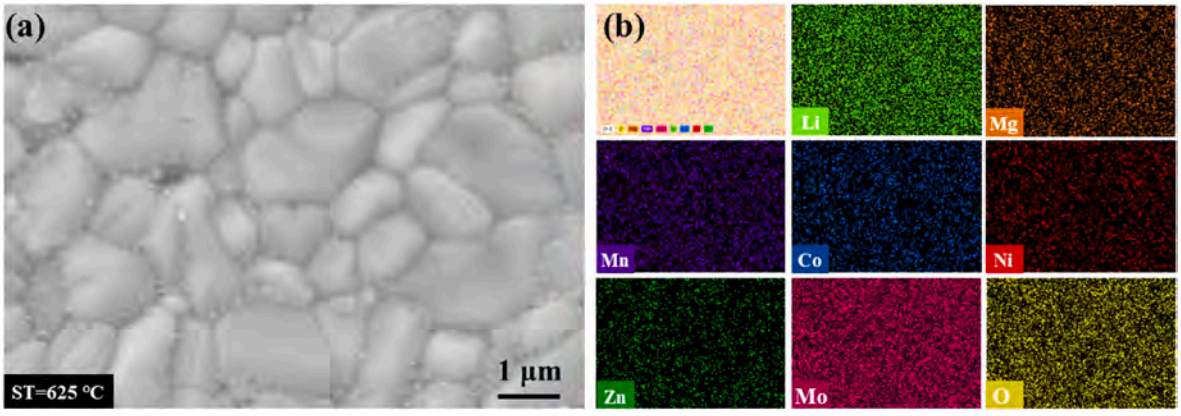

Fig. 3. SEM photo and EDS energy spectrum detection of LAM ceramics sintered at 625 °C.

P-V-L theory [29,30]:

$$f_i^{\mu} = \frac{(C^{\mu})^2}{\left(E_g^{\mu}\right)^2} = \frac{(C^{\mu})^2}{\left(E_h^{\mu}\right)^2 + (C^{\mu})^2} \tag{4}$$

$$\left(E_h^{\mu}\right)^2 = \frac{39.74}{(d^{\mu})^{2.48}} \tag{5}$$

$$C^{\mu} = 14.4 b^{\mu} \exp\left(-k_s^{\mu} r_0^{\mu}\right)\left[\left(Z_A^{\mu}\right)^* - \frac{n}{m}\left(Z_B^{\mu}\right)^*\right] \Big/ r_0^{\mu} \tag{6}$$

where d^{μ} is the bond length and the polarization energy of the chemical bond (E_g^{μ}) is divided into an anisotropic part (C_{μ}) and a homopolar part (E_h^{μ}). $\left(Z_A^{\mu}\right)^*$ and $\left(Z_B^{\mu}\right)^*$ are the effective number of valence electrons on cation A and anion B, respectively:

$$U = \sum_{\mu}\left(U_{bc}^{\mu} + U_{bi}^{\mu}\right) \tag{7}$$

$$U_{bc}^{\mu} = 2100 m \frac{\left(Z_{+}^{\mu}\right)^{1.64}}{\left(d^{\mu}\right)^{0.75}} f_i^{\mu} \tag{8}$$

$$U_{bi}^{\mu} = \frac{1270(m+n) Z_{+}^{\mu} Z_{-}^{\mu}}{d^{\mu}}\left(1 - \frac{0.4}{d^{\mu}}\right) f_i^{\mu} \tag{9}$$

where U_{bc}^{μ} and U_{bi}^{μ} represent the covalent and ionic parts of the lattice energy, respectively, and Z_{-}^{μ} and Z_{+}^{μ} represent the valence states of the ions. Fig. 4 demonstrates the average ionicity and lattice energy percentage of each bond of LAM ceramics at 625 °C. From the figure, it can be found that the ionicity and lattice energy of the Li/A-O bond are significantly lower than those of the Mo-O bond, which indicates that the influence of the Mo-O bond on the microwave dielectric properties dominates.

It is well known that the microwave dielectric properties of ceramic specimens are affected by a variety of external factors including, but not limited to, variations in porosity, second phase and grain size [31]. In order to avoid the influence of external factors on the dielectric constant as much as possible, Eq. (11) was used to correct the relative dielectric constant [32,33]:

$$\varepsilon_{corr} = \varepsilon_r(1 + 1.5P) \tag{10}$$

where P is the porosity, ρ_{rel} is the relative density of the ceramic sample, and ε_r and ε_{corr} are the relative permittivity (results are shown in Table S1) and the porosity-corrected permittivity (results are shown in Fig. 5), respectively. Fig. 5 shows ε_{corr} and f_i for LAM ceramics. ε_{corr} varies in much the same way as f_i, and the following relationship exists between the two [34]:

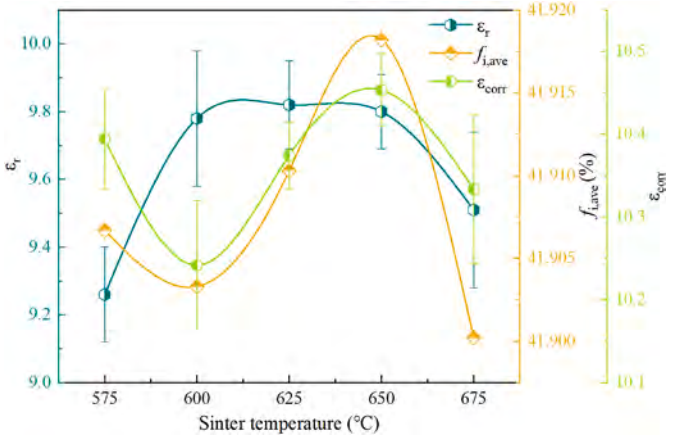

Fig. 5. Dielectric constant (ε_r), pore-corrected dielectric constant (ε_{corr}) and f_i of LAM ceramics at various sintering temperatures.

$$\varepsilon_r = \frac{n_r^2 - 1}{1 - f_i} + 1 \tag{11}$$

where nr is the refractive index. The P-V-L theory is studied for crystals, and idealized crystals do not have pores. So when the P-V-L theory is applied to the study of ceramic materials, the relative constant (ε_r) often represents the Pore-corrected dielectric constant (ε_{corr}). The more ionic the chemical bond, the stronger the polarization of the bond and the higher the corresponding dielectric constant.

The bond-averaged ionicity and lattice energy calculations for LAM ceramics at all sintering temperatures are shown in Figs. 5 and 6.

Fig. 6 shows the variation of quality factor ($Q \times f$), U and relative density of LAM ceramics at different sintering temperatures. From the figure, it can be found that the $Q \times f$ firstly increases from 18,434 GHz to 21,460 GHz and then decreases to 18,025 GHz, and the relative densities firstly increase and then decrease, and all of them are above 92 %. The trends of the $Q \times f$ and the relative densities are more or less the same, but there is a big difference in the trends of $Q \times f$ and relative density at the sintering temperature of 650 °C. This is due to the decrease of the lattice energy. On the one hand, it is due to the decrease of lattice energy, which leads to the great difference in the trends of the two. The higher the lattice energy, the more stable the crystal structure is, and the corresponding $Q \times f$ value is higher. On the other hand, it is due to changes in the grain size. When the average grain size increases and the number of grain boundaries decreases, the degree of phonon scattering at the grain boundaries is reduced, which helps to improve the $Q \times f$ value. However, an abnormal increase in grain size will deteriorate the $Q \times f$ value, which is caused by an excessively high ceramic sintering temperature. Fig. 2 shows that when ST > 625 °C, the grain dispersion

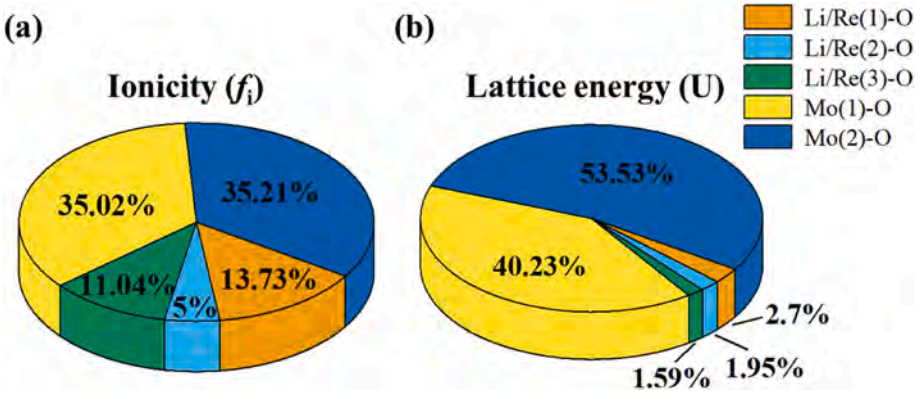

Fig. 4. Percentage of f_i and U for each chemical bond for sintered LAM ceramics at 625 °C.

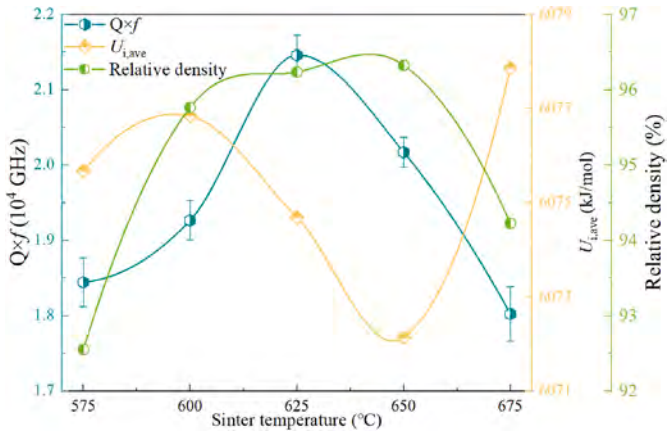

Fig. 6. Quality factor (Q × *f*), U and relative density of LAM ceramics at various sintering temperatures.

increases rapidly, which negatively affects the Q × *f* value.

The resonant frequency temperature coefficient (τ_f) is a key parameter of microwave dielectric ceramics, which determines the temperature stability of microwave dielectric ceramics [35]. In this study, the resonant frequency temperature coefficient of LAM ceramics is examined, and τ_f floats between −76.19 and −61.11 ppm/°C. The results are shown in Fig. 7. To further analyze the influencing factors of τ_f, the total bond valence ($V_{ij\text{-total}}$) and [Li/AO_6] oxygen octahedral average torsion (Δ_{oct}) were calculated using Eqs. (13)–(15) [36,37]:

$$V_{ij-total} = \sum v_{ij} \tag{12}$$

$$v_{ij} = \exp\left(\frac{R_{ij} - d_{ij}}{n}\right) \tag{13}$$

$$\Delta_{oct} = \frac{1}{6}\sum\left(\frac{R_{i-O} - R_{ave}}{R_{ave}}\right)^2 \tag{14}$$

where v_{ij} is the bond valence of ion i and ion j forming an ionic bond; d_{ij} is the bond length; R_{ij} is the bond valence parameter; n is the constant 0.37; R_i-O is the bond lengths of atoms i and O in the [Li/AO_6] oxygen octahedron, and Rave the average bond lengths, and the results of the calculations are shown in Fig. 7. The variation trend of Δ_{oct} is basically the same as that of τ_f, while $V_{ij\text{-total}}$ and τ_f show a negative correlation. The relationship between the change of Δ_{oct} and τ_f is in general agreement with the results of Li et al. [38]. The bond valence theory indicates [36] that the higher the bond valence, the higher the energy required to

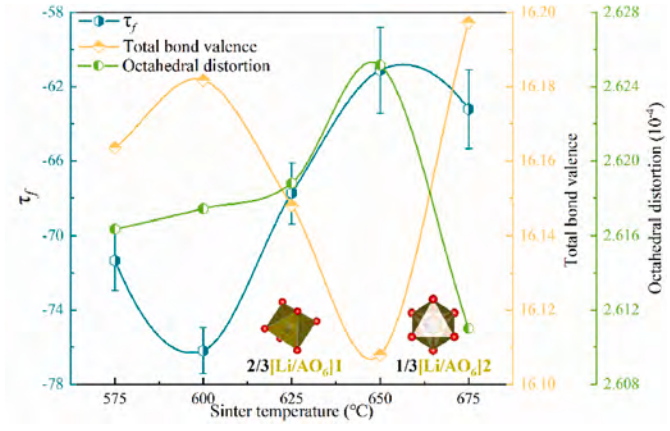

Fig. 7. Temperature coefficient of resonance frequency (τ_f), total bond valence ($V_{ij\text{-total}}$), and oxygen octahedral average torsion (Δ_{oct}) of LAM ceramics at various sintering temperatures.

recover the oxygen polyhedral deformation, which ultimately leads to a decrease in τ_f, which is consistent with the results of this study. At a sintering temperature of 675 °C, the magnitude of τ_f change in LAM ceramics is significantly different from the magnitude of $V_{ij\text{-total}}$ and Δ_{oct} change, which may be due to the high sintering temperature.

Table 2 demonstrates the ULTCC materials reported in recent years. The LAM ceramics in this work have high Q × *f* values and more near-zero τ_f compared to the reported ULTCC materials with low dielectric constants. It can be seen that the LAM ceramics are very promising candidates for ULTCC.

Fig. 8 (a, b) shows the comparison of the Vickers hardness and compressive strength of LAM ceramics and $Li_2Mg_2Mo_3O_{12}$ ceramics at each sintering temperature. The H_v and σ of LAM and $Li_2Mg_2Mo_3O_{12}$ ceramics both show a trend of first increasing and then decreasing as the sintering temperature rises. When the sintering temperature is 575 °C, the H_v and σ of the LAM ceramics are the minimum values, which are 2.54 GPa and 300 MPa, respectively. When the sintering temperature is raised to 625 °C, the H_v and σ of the LAM ceramics reach their maximum values, which are 4.54 GPa and 441 MPa, respectively. As the sintering temperature of the LAM ceramics is further increased, both the H_v and σ decrease. From the figure, it can be seen that the H_v and σ of LAM ceramics are significantly higher than those of $Li_2Mg_2Mo_3O_{12}$ ceramics. The Mg sites in LAM ceramics are occupied by ions with five different ionic radii, which will inevitably cause severe lattice distortion, thereby hindering the strain inside the lattice under external forces, suppressing transgranular fracture, and improving the mechanical properties of LAM ceramics. This is due to the severe lattice distortion effect caused by the high entropy LAM ceramic.

The H_v and σ of the LAM ceramics follow much the same trend as the relative densities, but there is a significant difference at the sintering temperature of 650 °C. According to Hall-Petch relationship [45,46], the following relationship exists between yield strength and grain size:

$$\sigma_y = \sigma_0 + k \cdot G^{-\frac{1}{2}} \tag{15}$$

where σ_y denotes the yield limit of the material, representing the value of the stress at which 0.2 % permanent residual deformation of the material occurs, σ_0 denotes the lattice frictional resistance, *k* is a constant, and G is the average grain size of the sample. Ehre et al. [47] showed that the hardness can be used in place of the σ_y, which also conforms to the Hall-Petch relationship. It can be seen that the inconsistency between the change in relative density and mechanical properties at a sintering temperature of 650 °C is due to the increase in grain size at this sintering temperature. According to Eq. 16, the larger the grain size, the worse the mechanical properties. The smaller the grain size, the more the proportion of grain boundaries in ceramics, the more the dislocations will be hindered by the grain boundaries during their movement, and the greater the stress required for the corresponding dislocation slip.

4. Conclusions

High entropy design is used to improve the mechanical properties of

Table 2
Microwave dielectric properties and sintering temperature (S.T.) of ULTCC materials.

Sample	ε_r	Q×*f* (GHz)	τ_f (ppm/C)	S.T.	Ref.
$ZnO\text{-}B_2O_3$	6.09	20,389	14	640 °C	[12]
$Cu_3Mo_2O_9$	7.20	19,300	−8	660 °C	[39]
$Li_2O\text{-}CoO\text{-}WO_3$	8.42	18,500	−46	600 °C	[40]
$3Li_2O\text{-}Bi_2O_3\text{-}6P_2O_5$	6.80	16,900	−71	625 °C	[41]
$CuO\text{-}B_2O_3\text{-}Li_2O$	5.84	10,120	−33	625 °C	[42]
$CaO\text{-}ZnO\text{-}B_2O_3\text{-}P_2O_5$	4.32	16,820	−27	740 °C	[43]
$BiZn_2VO_6$	8.90	13,000	−97	600 °C	[44]
LAM	9.82	21,460	−68	625 °C	This work

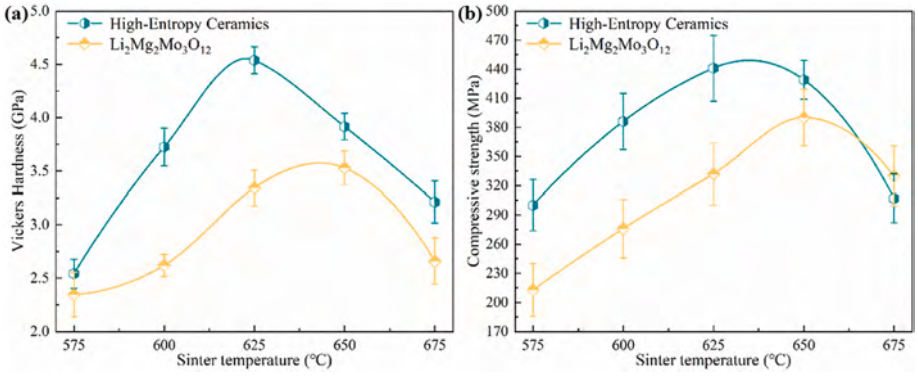

Fig. 8. Comparison of mechanical properties of LAM ceramics and $Li_2Mg_2Mo_3O_{12}$ ceramics at various sintering temperatures. (a) Vickers hardness, H_v (b) Compressive strength, σ.

LAM ceramics. The results show that the best mechanical properties of LAM ceramics (H_v = 4.54 GPa, σ = 441 MPa) are significantly better than the best mechanical properties of $Li_2Mg_2Mo_3O_{12}$ ceramics (H_v = 3.53 GPa, σ = 390 MPa). This suggests that it is feasible to use high entropy design to improve the mechanical property performance method in LAM ceramics. In addition to this, the microwave dielectric properties of LAM ceramics were investigated and the best microwave dielectric properties of LAM ceramics were obtained when ST = 625 °C (ε_r = 9.82, Q × f = 20,514 GHz, τ_f = −67.74 ppm/°C). The microwave dielectric properties of LAM ceramics are strongly influenced by external factors, especially the relative density and grain size. The results show that the effect of Mo-O bonds on the microwave dielectric properties is significantly higher than that of Li/A-O bonds. ε_{corr} floats are mainly attributed to the change in the average f_i of the bonds, and the decrease in the Q × f value of the LAM ceramics at ST = 650 °C is due to the decrease in U. The floating of τ_f is mainly due to $V_{ij\text{-}total}$ variation.

CRediT authorship contribution statement

Yutong Meng: Writing – original draft, Formal analysis, Data curation. **Qi Yuan:** Writing – original draft, Formal analysis, Data curation. **Sen Wang:** Writing – review & editing, Project administration.

Declaration of competing interest

No conflict of interest exists in the submission of this manuscript, and the manuscript has been approved by all authors for publication. I would like to declare on behalf of my co-authors that the work described was original research that has not been published previously or is under consideration for publication elsewhere, in whole or in part. All the authors listed have approved the manuscript that is enclosed.

Appendix A. Supplementary data

Supplementary data to this article can be found online at https://doi.org/10.1016/j.ceramint.2025.05.213.

References

[1] J. Zhou, Towards rational design of low-temperature co-fired ceramic (LTCC) materials, J. Adv. Ceram. 1 (2012) 89–99, https://doi.org/10.1007/s40145-012-0011-3.

[2] D.A. Vinnik, V.E. Zhivulin, D.P. Sherstyuk, A.Y. Starikov, P.A. Zuzina, S. A. Gudkova, D.A. Zherebtsov, K.N. Rozanov, S.V. Trukhanov, K.A. Astapovich, V. A. Turchenko, A.S.B. Sombra, D. Zhou, R.B. Jotania, C. Singh, A.V. Trukhanov, Electromagnetic properties of zincenickel ferrites in the frequency range of 0.05e10 GHz, Mater. Today Chem. 20 (2012) 100460, https://doi.org/10.1016/j.mtchem.2021.100460.

[3] A. Hajian, A. Artemenko, A. Kromka, S. Schwarz, M. Schneider, K. Dragounová, M. Adaikkan, C. Zellner, U. Schmid, Impact of sintering temperature on phase composition, microstructure, and porosification behavior of LTCC substrates, J. Eur. Ceram. Soc. 42 (2022) 5789–5800, https://doi.org/10.1016/j.jeurceramsoc.2022.05.049.

[4] X.M. Li, X. Xue, H. Wang, J. Guo, Recent development on ultra-low firing technologies of microwave dielectric ceramics, J. Chinese, Ceram. Soc. 51 (2023) 907–920, https://doi.org/10.14062/j.issn.0454-5648.20220700.

[5] M.T. Sebastian, H. Jantunen, High temperature cofired ceramic (HTCC), low temperature cofired ceramic (LTCC), and ultralow temperature cofired ceramic (ULTCC) materials, MW, Mater. Appl. 5 (2017) 355–425, https://doi.org/10.1002/9781119208549.ch8.

[6] J. Varghese, P. Ramachandran, M. Sobocinski, T. Vahera, H. Jantunen, ULTCC glass composites based on rutile and anatase with cofiring at 400° C for high frequency applications, ACS Sustain. Chem. Eng. 7 (2019) 4274–4283, https://doi.org/10.1021/acssuschemeng.8b06048.

[7] S.Z. Hao, D. Zhou, F. Hussain, J.Z. Su, W.F. Liu, D.W. Wang, Q.P. Wang, Z.M. Qi, Novel scheelite-type $[Ca_{0.55}(Nd_{1-x}Bi_x)_{0.3}]MoO_4$ ($0.2 \leq X \leq 0.95$) microwave dielectric ceramics with low sintering temperature, J. Am. Ceram. Soc. 103 (2020) 7259–7266, https://doi.org/10.1111/jace.17378.

[8] J. Ren, K. Bi, X. Fu, Z. Peng, Novel Bi_2O_3-added $Al_2Mo_3O_{12}$ composite microwave dielectric ceramics for ULTCC applications, J. Alloys Compd. 823 (2020) 153867, https://doi.org/10.1016/j.jallcom.2020.153867.

[9] T.H. Hsu, C.L. Huang, Low-loss microwave dielectric of novel $Li_{1-2x}M_xVO_3$ (M= Mg, Zn)(x= 0–0.09) ceramics for ULTCC applications, J. Eur. Ceram. Soc. 41 (2021) 5918–5923, https://doi.org/10.1016/j.jeurceramsoc.2021.05.033.

[10] J. Varghese, P. Ramachandran, M. Sobocinski, T. Vahera, H. Jantunen, ULTCC glass composites based on rutile and anatase with cofiringat 400 °C for high frequency applications, ACS Sustainable Chem. Eng. 7 (2019) 4274–4283, https://doi.org/10.1021/acssuschemeng.8b06048.

[11] S. Chen, L.K. Liu, W. Li, Sintering behavior and dielectric properties of ultra-low temperature glass/ceramic composites, Mater. Res. Bull. 114 (2019) 107–111, https://doi.org/10.1016/j.materresbull.2019.02.030.

[12] W. Gao, J. Zhang, C. Ji, L. Li, J. Wang, Chao Liu, Jian Ruan, J. Han, High-performance microwave dielectric glass-ceramic with fine secondary structure for ULTCC application, J. Eur. Ceram. Soc. 43 (2023) 2513–2522, https://doi.org/10.1016/j.jeurceramsoc.2023.01.004.

[13] D. Zhou, H. Wang, L.X. Pang, A.R. Clive, Y. Xi, Bi_2O_3–MoO_3 binary system: an alternative ultralow sintering temperature microwave dielectric, J. Am. Ceram. Soc. 92 (2009) 2242–2246, https://doi.org/10.1111/j.1551-2916.2009.03185.x.

[14] E.S. Kim, B.S. Chun, R. Freer, J.C. Robert, Effects of packing fraction and bond valence on microwave dielectric properties of $A^{2+}B^{6+}O_4$ (A^{2+}:Ca, Pb, Ba; B^{6+}:Mo, W) ceramics, J. Eur. Ceram. Soc. 30 (2010) 1731–1736, https://doi.org/10.1016/j.jeurceramsoc.2009.12.018.

[15] L.X. Pang, D. Zhou, J. Guo, Z.X. Yue, Y. Xi, Microwave dielectric properties of $(Li_{0.5}Ln_{0.5})MoO_4$ (Ln= Nd, Er, Gd, Y, Yb, Sm, and Ce) ceramics, J. Am. Ceram. Soc. 98 (2015) 130–135, https://doi.org/10.1111/jace.13247.

[16] G.K. Choi, J.R. Kim, S.H. Yoon, K.S. Hong, Microwave dielectric properties of scheelite (A=Ca, Sr, Ba) and wolframite (A=Mg, Zn, Mn) $AMoO_4$ compounds, J. Eur. Ceram. Soc. 27 (2007) 3063–3067, https://doi.org/10.1016/j.jeurceramsoc.2006.11.037.

[17] D. Zhou, C.A. Randall, L.X. Pang, W. Hong, X.G. Wu, G. Jing, G.Q. Zhang, S. Li, Y. Xi, Microwave dielectric properties of $Li_2(M^{2+})_2Mo_3O_{12}$ and $Li_3(M^{3+})Mo_3O_{12}$ (M=Zn, Ca, Al, and in) lyonsite-related-type ceramics with ultra-low sintering temperatures, J. Am. Ceram. Soc. 94 (2011) 802–805, https://doi.org/10.1111/j.1551-2916.2010.04148.x.

[18] L.X. Pang, G.B. Sun, D. Zhou, $Ln_2Mo_3O_{12}$ (Ln=La, Nd): a novel group of low loss microwave dielectric ceramics with low sintering temperature, Mater. Lett. 65 (2011) 164–166, https://doi.org/10.1016/j.matlet.2010.09.064.

[19] W. Bian, G. Zhou, Y. Dong, X. Lu, H. Zhu, S. Ta, L. Wang, Q. Zhang, Structural analysis and microwave dielectric properties of a novel $Li_2Mg_2Mo_3O_{12}$ ceramic with ultra-low sintering temperature, Ceram. Int. 47 (2021) 7081–7087, https://doi.org/10.1016/j.ceramint.2020.11.059.

[20] S. Kawai, S. Nishiura, Y. Terashi, T. Furuse, Development of LTCC materials with high mechanical strength, IOP Conf. Ser. Mater. Sci. Eng. 18 (2011) 1–4, https://doi.org/10.1088/1757-899X/18/9/092013.

[21] Y.Y. Zhang, L. Chen, H. Liu, S.Q. Deng, H. Qi, J. Chen, High-performance ferroelectric based materials via high-entropy strategy: design, properties, and mechanism, InfoMat (2023) 12488, https://doi.org/10.1002/inf2.12488.
[22] C. Toher, C. Oses, M. Esters, High-entropy ceramics: propelling applications through disorder, MRS Bull. 47 (2022) 194–202, https://doi.org/10.1557/s43577-022-00281-x.
[23] H.M. Xiang, Y. Xing, F.Z. Dai, H. Wang, L. Su, L. Miao, G. Zhang, Y. Wang, X. Qi, L. Yao, H. Wang, High-entropy ceramics: present status, challenges, and a look forward, J. Adv. Ceram. 10 (2021) 385–441, https://doi.org/10.1007/s40145-021-0477-y.
[24] C.A. Corlett, N. Obradovic, J.L. Watts, E.W. Bohannan, W.G. Fahrenholtz, Synthesis, densification, and cation inversion in high entropy (Co, Cu, Mg, Ni, Zn) Al_2O_4 spinel, J. Asian. Ceram. Soc. 11 (2023) 330–337, https://doi.org/10.1080/21870764.2023.2227535.
[25] L.L. Feng, L. Bing, C.H. Cheng, X.S. Kai, Novel high-entropy microwave dielectric ceramics $Sr(La_{0.2}Nd_{0.2}Sm_{0.2}Eu_{0.2}Gd_{0.2})AlO_4$ with excellent temperature stability and mechanical properties, J. Eur. Ceram. Soc. 43 (2023) 2506–2512, https://doi.org/10.1016/j.jeurceramsoc.2023.01.028.
[26] X.X. Xu, Z.Y. Wen, X.W. Wu, X.L. Yang, Z.H. Gu, Lithium ion-conducting glass–ceramics of $Li_{1.5}Al_{0.5}Ge_{1.5}(PO_4)_3$–$xLi_2O$ (x=0.0–0.20) with good electrical and electrochemical properties, J. Eur. Ceram. Soc. 90 (2007) 2802–2806, https://doi.org/10.1111/j.1551-2916.2007.01827.x.
[27] J. Qin, Z. Liu, M. Ma, Y. Li, Optimizing and extending ion dielectric polarizability database for microwave frequencies using machine learning methods, npj Comput. Mater. 9 (2023) 132, https://doi.org/10.1038/s41524-023-01093-6.
[28] Z. Qing, H. Zou, X. Zhou, H. Li, A. Liu, S. Duan, Y. Li, S. Peng, Crystal structures, chemical bond features, and Raman vibrations of $Li_2Co_2Mo_3O_{12}$ microwave dielectric ceramics with low sintering temperature, J. Am. Ceram. Soc. 107 (2024) 223–233, https://doi.org/10.1111/jace.19432.
[29] X.K. Lan, J. Li, Z.Y. Zou, G.F. Fan, W.Z. Lu, W. Lei, Lattice structure analysis and optimised microwave dielectric properties of $LiAl_{1-x}(Zn_{0.5}Si_{0.5})_xO_2$ solid solutions, J. Eur. Ceram. Soc. 39 (2019) 2360–2364, https://doi.org/10.1016/j.jeurceramsoc.2019.02.011.
[30] A.J. Bosman, E.E. Havinga, Temperature dependence of dielectric constants of cubic ionic compounds, Phys. Rev. 129 (1963) 1593–1600, https://doi.org/10.1103/PhysRev.129.1593.
[31] Z. Wu, S. Zhang, Semiempirical method for the evaluationof bond covalency in complex crystals, J. Phys. Chem. A 103 (1999) 4270–4274, https://doi.org/10.1021/jp982674q.
[32] S.J. Penn, N.M. Alford, A. Templeton, X. Wang, M. Xu, M. Reece, K. Schrapel, Effect of porosity and grain size on the microwave dielectric properties of sintered alumina, J. Am. Ceram. Soc. 80 (1997) 1885–1888, https://doi.org/10.1111/j.1151-2916.1997.tb03066.x.
[33] J. Bao, Y.P. Zhang, H.D. Kimura, H.T. Wu, Z.X. Yue, Crystal structure, chemical bond characteristics, infrared reflection spectrum, and microwave dielectric properties of $Nd_2(Zr_{1-x}Ti_x)_3(MoO_4)_9$ ceramics, J. Adv. Ceram. 12 (2023) 82–92, https://doi.org/10.26599/JAC.2023.9220668.
[34] S.S. Batsanov, Dielectric methods of studying the chemical bond and the concept of electronegativity, Russ. Chem. Rev. 51 (1982) 684, https://doi.org/10.1070/RC1982v051n07ABEH002900.
[35] L. Li, R. Ubic, X.M. Chen, On the τ_f measurement of microwave dielectric ceramics, Mater. Res. Bull. 178 (2024) 112920, https://doi.org/10.1016/j.materresbull.2024.112920.
[36] N.E. Brese, M. O'Keeffe, Bond-valence parameters for solids, Acta Crystallogr. B 47 (1991) 192–197, https://doi.org/10.1107/S0108768190011041.
[37] I.M. Reaney, E. Colla, N. Setter, Dielectric and struc-tural characteristics of Ba- and Sr-based complex perovskites as a function of tolerance factor, Jpn. J. Appl. Phys. 33 (1994) 3984, https://doi.org/10.1143/JJAP.33.3984.
[38] F. Li, Y. Li, Y. Li, X. Feng, J. Zhang, X. Liu, Y. Lu, S. Wang, Y. Liao, T. Tang, Q. Wen, Enhanced Na^+-substituted $Li_2Mg_2Mo_3O_{12}$ ceramic substrate based on ultra-low temperature co-fired ceramic technology for microwave and terahertz polarization-selective functions, J. Eur. Ceram. Soc. 43 (2023) 384–391, https://doi.org/10.1016/j.jeurceramsoc.2022.10.031.
[39] W.X. Wen, C.C. Li, Y.H. Sun, Y. Tang, L. Fang, $Cu_3Mo_2O_9$: an ultralow-firing microwave dielectric ceramic with good temperature stability and chemical compatibility with aluminum, J. Electron. Mater. 47 (2018) 1003–1008, https://doi.org/10.1007/s11664-017-5957-z.
[40] C.F. Tseng, C.H. Chiang, P.H. Chen, S.Y. Chang, T.L. Chuang, Ultra-low temperature fired glass-free Li_2O-MO-WO_3 (M = Co, Ni, Ca, Ba) microwave dielectric ceramics, J. Mater. Sci. Mater. Electron. 29 (2018) 14835–14841, https://doi.org/10.1007/s10854-018-9620-0.
[41] X.B. Liu, S.H. Yang, H.Q. Wang, K.G. Wang, X.L. Xie, H.F. Zhou, New lithium bismuth phosphate ceramic: crystal structure, microstructure, microwave dielectric properties and co-firing compatibility with aluminum electrode, J. Mater. Sci. Mater. Electron. 22 (2022) 8001–8006, https://doi.org/10.1007/s10854-022-08001-6.
[42] M. Ma, Z. Fu, Z. Liu, Y. Li, Fabrication and microwave dielectric properties of CuO-B_2O_3-Li_2O glass-ceramic with ultra-low sintering temperature, Ceram. Int. 43 (2017) S292–S295, https://doi.org/10.1016/j.ceramint.2017.05.190.
[43] D.H. Jiang, J.J. Chen, B.B. Lu, J. Xi, G.H. Chen, A new glass-ceramic with low permittivity for LTCC application, J. Mater. Sci. Mater. Electron. 29 (2018) 18426–18431, https://doi.org/10.1007/s10854-018-9957-4.
[44] H. Xiang, Y. Bai, J. Varghese, C. Li, L. Fang, H. Jantunen, Ultralow temperature cofired $BiZn_2VO_6$ dielectric ceramics doped with B_2O_3 and Li_2CO_3 for ULTCC applications, J. Am. Ceram. Soc. 102 (3) (2019) 1218–1226, https://doi.org/10.1111/jace.15953.
[45] E.O. Hall, The deformation and ageing of mild steel: III discussion of results, P. Phy, Soc. Section B 64 (1951) 747–752, https://doi.org/10.1088/0370-1301/64/9/303.
[46] N.J. Petch, The cleavage strength of polycrystals, J. Iron. Steel. Inst. 174 (1953) 25–28, https://doi.org/10.1299/kikaia.74.412.
[47] D. Ehre, R. Chaim, Abnormal hall–petch behavior in nanocrystalline MgO ceramic, J. Mater. Sci. 18 (2008) 6139–6143, https://doi.org/10.1007/s10853-008-2936-z.